PHILOSOPHICAL TRANSACTIONS A

rsta.royalsocietypublishing.org

Research

Cite this article: Brahimi SV, Yue S, Sriraman KR. 2017 Alloy and composition dependence of hydrogen embrittlement susceptibility in high-strength steel fasteners. *Phil. Trans. R. Soc. A* **375**: 20160407.
http://dx.doi.org/10.1098/rsta.2016.0407

Accepted: 18 April 2017

One contribution of 24 to a discussion meeting issue 'The challenges of hydrogen and metals'.

Subject Areas:
materials science

Keywords:
high-strength fasteners, hydrogen embrittlement susceptibility, tempered martensite, cathodic charging, internal hydrogen embrittlement, environmental hydrogen embrittlement

Author for correspondence:
S. V. Brahimi
e-mail: salim.brahimi@mcgill.ca

Electronic supplementary material is available online at https://dx.doi.org/10.6084/m9.figshare.c.3778853.

THE ROYAL SOCIETY PUBLISHING

Downloaded from https://royalsocietypublishing.org/ on 04 March 2022

Alloy and composition dependence of hydrogen embrittlement susceptibility in high-strength steel fasteners

S. V. Brahimi[1,2], S. Yue[1] and K. R. Sriraman[1]

[1]Department of Mining and Materials Engineering, McGill University, Montreal, QC H3A 0E8, Canada
[2]Industrial Fasteners Institute, Cleveland, OH 44131, USA

High-strength steel fasteners characterized by tensile strengths above 1100 MPa are often used in critical applications where a failure can have catastrophic consequences. Preventing hydrogen embrittlement (HE) failure is a fundamental concern implicating the entire fastener supply chain. Research is typically conducted under idealized conditions that cannot be translated into know-how prescribed in fastener industry standards and practices. Additionally, inconsistencies and even contradictions in fastener industry standards have led to much confusion and many preventable or misdiagnosed fastener failures. HE susceptibility is a function of the material condition, which is comprehensively described by the metallurgical and mechanical properties. Material strength has a first-order effect on HE susceptibility, which increases significantly above 1200 MPa and is characterized by a ductile–brittle transition. For a given concentration of hydrogen and at equal strength, the critical strength above which the ductile–brittle transition begins can vary due to second-order effects of chemistry, tempering temperature and sub-microstructure. Additionally, non-homogeneity of the metallurgical structure resulting from poorly controlled heat treatment, impurities and non-metallic inclusions can increase HE susceptibility of steel in ways that are measurable but unpredictable. Below 1200 MPa, non-conforming quality is often the root cause of real-life failures.

This article is part of the themed issue 'The challenges of hydrogen and metals'.

© 2017 The Author(s) Published by the Royal Society. All rights reserved.

Downloaded from https://royalsocietypublishing.org/ on 04 March 2022

1. Introduction

(a) General description of hydrogen embrittlement in high-strength steel

Hydrogen embrittlement (HE) causes loss of ductility and, consequently, a loss of strength. HE in high-strength steel is described as permanent loss of ductility in a metal or alloy caused by atomic hydrogen in combination with load-induced and/or residual tensile stress that can lead to brittle fracture after a certain time [1]. Generally, HE is classified under two broad categories based on the source of hydrogen: internal hydrogen embrittlement (IHE) and environmental hydrogen embrittlement (EHE). In the context of mechanical fasteners, IHE is caused by residual hydrogen that is introduced during manufacturing before the fastener is tensioned and put into service. Potential manufacturing sources of 'internal' hydrogen range from steelmaking to heat treatment and finally to surface finishing. Electroplating, typically to deposit zinc or zinc alloys for corrosion protection, is the single most consequential process with respect to IHE. This is not only because electroplating is the last manufacturing process where hydrogen is introduced, but also hydrogen that is absorbed during surface preparation (e.g. acid pickling) followed by electroplating is 'locked-in' by the coating metal, which acts as a barrier to hydrogen effusion from the finished fastener [2,3]. EHE is caused by hydrogen introduced into the fastener from external sources while it is in use and under stress. The term 'stress corrosion cracking' (SCC) is used to describe EHE that occurs when hydrogen is produced as a by-product of surface corrosion. Cathodic hydrogen absorption, a subset of SCC, occurs in the presence of metallic coatings such as zinc or cadmium that are designed to sacrificially oxidize to protect a steel substrate from corrosion. If the underlying substrate becomes exposed, a reduction reaction on the exposed steel surface simultaneously results in the evolution of hydrogen in quantities that are significantly greater than for uncoated steel.

When a high-strength fastener is tensioned, a stress concentration gradient causes atomic hydrogen to migrate to locations of greatest stress. For a threaded bolt these locations are the first engaged thread and at the head–body junction. As higher concentrations of hydrogen collect at these locations, steel that is normally ductile transitions to being brittle. Eventually, the concentration of stress and hydrogen in one location causes a brittle microcrack. The microcrack continues to grow as hydrogen moves to follow the tip of the propagating crack, until the fastener is overloaded and finally fractures. This phenomenon is often called hydrogen-assisted cracking (HAC) or hydrogen-induced cracking (HIC). The mechanism of hydrogen damage causes the fastener to fail at stresses that are significantly lower than its basic material strength as determined by a standard tensile test [4,5].

Theoretical models that describe hydrogen damage mechanisms under idealized conditions have been proposed since the 1960s. In the specific context of high-strength steel, these models are based on two complementary theories of decohesion [6,7] and hydrogen-enhanced local plasticity (HELP) [8,9]. Given the complexity of HE phenomena, hydrogen damage models continue to evolve and be refined [10].

Hydrogen 'traps' refer to metallurgical features within the steel microstructure, such as grain boundaries, dislocations, precipitates, inclusions, etc., to which hydrogen atoms may become bonded. Hydrogen thus 'trapped' is no longer free to diffuse to areas of high stress where it can participate in the mechanism of HAC. Traps are typically classified as reversible or non-reversible based on their bonding energies. Reversible traps are characterized by low bonding energies: in other words, hydrogen is more easily released from the trap. Non-reversible traps are characterized by high bonding energies: in other words, hydrogen requires a great deal of energy (e.g. heat) to be released from the trap. Non-trapped hydrogen which is free to move in the metal lattice is called mobile hydrogen; it also known as interstitial or diffusible hydrogen [11].

Three conditions must be met to cause HE failure in high-strength steel (figure 1):

(i) material condition that is susceptible to hydrogen damage,

Downloaded from https://royalsocietypublishing.org/ on 04 March 2022

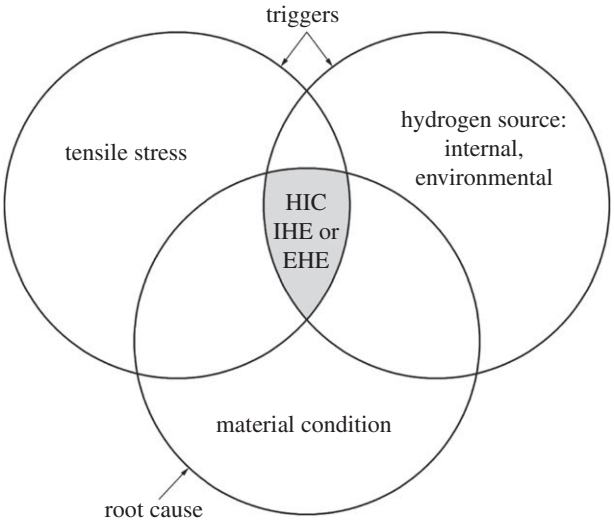

Figure 1. Given time, three conditions must be met in sufficient and overlapping quantities for hydrogen embrittlement (HE) failure to occur. Stress and hydrogen are triggers, whereas material susceptibility is the fundamental requirement for HE to occur and is therefore associated with the root cause.

(ii) tensile stress (typically from an externally applied load or residual stresses) and
(iii) atomic hydrogen.

If all three of these elements are present in sufficient quantities, and given *time*, hydrogen damage results in crack initiation and growth until the occurrence of fracture. Time to failure can vary, depending on the severity of the conditions and the source of hydrogen [4,5,12–15].

(b) Material susceptibility

HE susceptibility is a function of the material condition, which is comprehensively described by the metallurgical and mechanical properties of a material such as steel. Therein lies the fundamental basis for understanding HE phenomena, which, when simply stated, is the study of how a material performs in the absence and then in the presence of absorbed hydrogen. Material strength (i.e. tensile strength and/or hardness) has a first-order effect on HE susceptibility. As strength increases, steel becomes harder, less ductile, less tough and more susceptible to HE.

The susceptibility of quenched and tempered (i.e. martensitic) steel increases significantly above 1200 MPa (approx. 39 HRC, 390 HV) [13].

Important considerations in the prevention of HE are the selection and heat treatment of materials used to manufacture threaded fasteners. Typically, fastener specifications mandate mechanical performance while only placing broad restrictions on material selection. In other words, standard specifications do not mandate the selection of a specific alloy. The final material condition of high-strength steel fasteners is obtained by the heat treatment process (i.e. quenching and tempering). Heat treatment is the most consequential process for obtaining the required mechanical and metallurgical properties. Fortunately, fastener failures by the mechanism of HE are not common. In rare cases where such a failure does occur, the *root cause* is linked either to incorrect selection of a fastener for a given application or to a manufacturing defect, typically improper heat treatment. Consequences of improper heat treatment include higher-than-expected hardness, unintended carburization and incomplete martensite transformation, all of which can cause higher-than-expected susceptibility to hydrogen damage. Therefore, it is imperative the heat treatment process produce a homogeneous and controlled microstructure [16].

Another material factor that can lead to higher-than-expected susceptibility to hydrogen damage is steel cleanliness characterized principally by inclusion content. High concentrations

Downloaded from https://royalsocietypublishing.org/ on 04 March 2022

of endogenous inclusions, such as MnS stringers in high-manganese alloys, or abnormally high concentrations of large acicular exogenous inclusions, such as those caused by refractory contamination during steel casting, become hydrogen traps that can increase the susceptibility of steel to hydrogen damage [17–19].

(c) Objective

This paper is part of a larger body of work aimed at better defining the relationship between chemical composition, microstructural characteristics and HE susceptibility of high-strength steel used for manufacturing mechanical fasteners. It is generally understood that strength and/or hardness have a first-order effect on HE susceptibility in high-strength steel. In this work, testing and observations made on nine alloys, each quenched and tempered to four hardness levels, illustrate second-order differences in susceptibility that are dependent on chemistry and heat treatment, and ultimately on microstructure.

2. Materials and methods

(a) Methodology

This study begins with testing aimed at measuring the susceptibility of materials to HE by comparing their behaviour first without added hydrogen (i.e. testing in air) and then with the addition of hydrogen under imposed cathodic potential. The principal investigative technique used is mechanical testing by incremental step loading (ISL) modelled on test method ASTM F1624 [20]. In brief, this approach consists of performing an incremental bending test on a notched square bar specimen. The test methodology is designed to measure the HE cracking threshold of the material.

The addition of hydrogen in the sample is achieved in an environmental chamber where the sample is immersed in 3.5 wt% NaCl solution. A potentiostat is used to impose the cathodic potential similar in principle to cathodic protection systems. The imposed potential and the resulting current density control the quantity of hydrogen being introduced into the specimen. The potential is varied from −1.20 V to −0.70 V versus saturated calomel electrode (SCE). The most severe hydrogen charging condition occurs at −1.20 V, which effectively reproduces the condition of sacrificial anodic protection by zinc. The least severe condition occurs at −0.70 V, which is just below the equilibrium corrosion potential of steel. The susceptibility of the material is expressed by per cent notch fracture strength ($NFS_{\%}$), which is defined as

$$NFS_{\%1.2V} = \frac{ISL_{1.2V}}{FF}, \tag{2.1}$$

where $NFS_{\%1.2V}$ is per cent notch fracture strength at an imposed potential of −1.20 V; FF is fast fracture load in air (baseline), 445 N min^{-1}; and $ISL_{1.2V}$ is minimum notch fracture load of specimen at an imposed potential of −1.20 V, ISL loading rate.

The duration of each test can vary from 5 to 80 h and is dependent upon the loading rate and the degree of embrittlement of the specimen. These loading protocols are defined by step patterns comprising 1, 2 or 3 h steps at 5% or 2% $NFS_{\%}$ load increments. Specimens of the same group are tested at progressively decreased loading rates, until the minimum or *invariant* value of stress or load is established. This process of establishing the invariant stress value is a function of the time dependence of HE. If the invariant stress has been correctly determined, by definition, reducing the loading rate will not yield a lower fracture stress.

(b) Test specimens

The materials are tested in the form of specimens, more precisely, single edge-notched square bars made from each material, machined to the dimensions of ASTM F519 type 1e (figure 2).

Downloaded from https://royalsocietypublishing.org/ on 04 March 2022

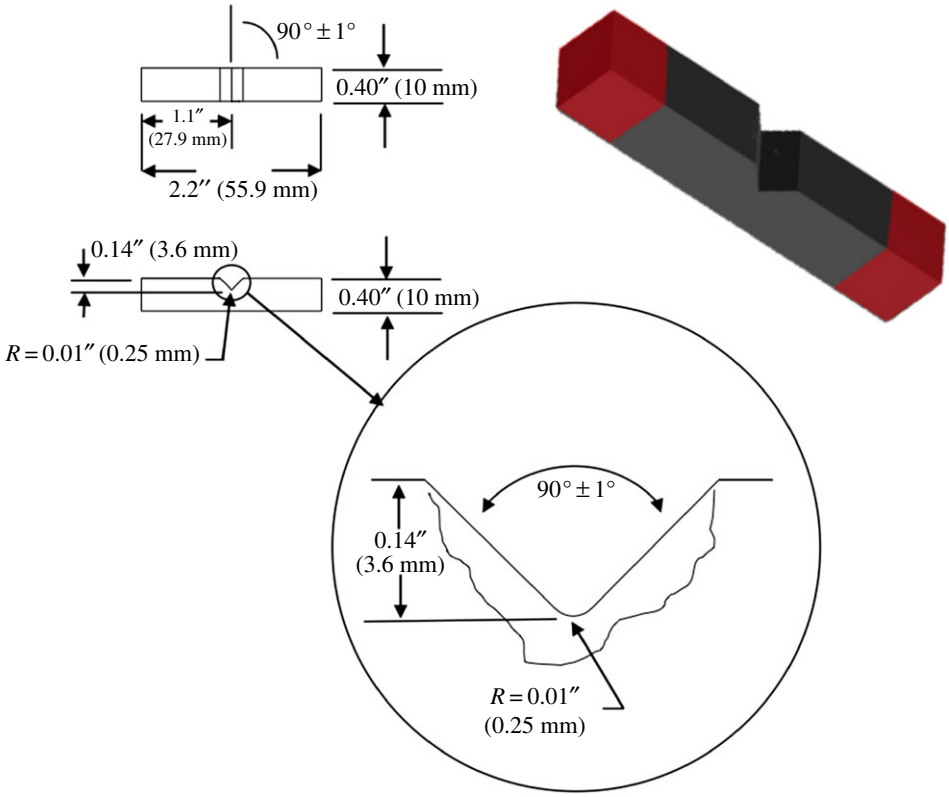

Figure 2. Dimensions of ASTM F519 (type 1e) single edge-notched bend square bar specimen. (Online version in colour.)

The predicted stress concentration factor K_t for this specimen geometry is 4.27 ± 0.32 [21]. This geometry is designed for applying load in four-point bending with the advantage of increasing the stress in the notch by an estimated factor of 1.6 when compared to testing in pure tension. Interpretation of results in the context of fasteners must be preceded by a correction for the increased stress, given that fasteners are loaded in tension and not in bending.

Test specimens are manufactured from raw material by cutting steel rod into square-shaped blanks in the rolling direction. The blanks are quenched and tempered to achieve target hardness levels. The notch is rough machined by wire electrical discharge machining within 0.5 mm of the final notch depth. Final notch depth and specimen dimensions are produced by low-stress grinding. The surface finish of the notch is 0.4 µm root mean square or better. No chemical or mechanical cleaning is performed after final machining. The last manufacturing step consists of a stress relief at 190°C for approximately 4 h. The specimens are then coated with light oil to prevent corrosion during storage. Prior to environmental testing, the specimens are cleaned with acetone and wiped to remove any surface residue or oxidation.

(c) Materials

Nine different steel alloys typically used for manufacturing high-strength fasteners were selected for this study (tables 1 and 2). The materials were quenched and tempered to achieve approximately equal hardness at four target hardness levels (i.e. 35, 39, 45, 53 HRC). Higher alloying content has the consequence of increasing as-quenched hardness and subsequently requiring higher tempering temperatures to achieve the same final hardness. Calculated carbon equivalents (CE) are shown in figure 3. Specific heat treatment conditions are given in the electronic supplementary material.

Downloaded from https://royalsocietypublishing.org/ on 04 March 2022

Table 1. Alloy designations and lot designations by hardness group. Bold values indicate alloys selected for in-depth microstructural evaluation.

		lot number			
alloy number	AISI designation	35 HRC	39 HRC	45 HRC	53 HRC
A1	8640H SiAK	M15	M3	M7	M11
A2	**5140 SK V**	**M16**	M4	M8	**M12**
A3	4042M SK V	M17	M5	M9	M13
A4	10B38M SiAK	M18	M6	M10	M14
A6	**4135MLV**	**M23**	M24	M25	**M26**
A7	1039	M35	M36	M37	M38
A8	10B21	M27	M28	M29	M30
A9	4340 per AMS-6414 (Vac Melt)	M19	M20	M21	M22
B1	4340 per MIL-S-5000 (Air Melt)	M31	M32	M33	M34

Table 2. Chemical composition for each alloy by weight per cent.

	A1-8640H	A2-5140	A3-4042M	A4-10B38M	A5-4135MLV AR	A7-1039 AR	A8-10B21	A9-4340 Vac	B1-4340 Air
C	0.41	0.40	0.43	0.39	0.35	0.41	0.19	0.40	0.41
Mn	0.88	0.75	0.92	0.83	0.9	0.89	0.84	0.78	0.77
P	0.009	0.011	0.011	0.013	0.010	0.014	0.004	0.005	0.007
S	0.001	0.018	0.017	0.003	0.015	0.017	0.006	0.002	0.003
Si	0.26	0.21	0.20	0.27	0.25	0.22	0.17	0.23	0.22
Cu	0.06	0.14	0.12	0.18	0.06	0.10	—	0.15	0.18
Ni	0.42	0.04	0.04	0.06	0.04	0.04	—	1.74	1.72
Cr	0.44	0.76	0.25	0.09	0.95	0.06	—	0.80	0.82
Mo	0.170	0.013	0.220	0.020	0.16	0.01	—	0.27	0.28
Al	0.037	0.001	0.001	0.03	0.001	0.002	0.043	0.013	0.016
V	0.002	0.023	0.022	—	0.02	0.002	—	0.001	0.001
B	—	—	—	0.0016	—	—	0.0018	—	—

3. Results

Results presented here were obtained over a period of three years of intensive testing, owing to the slow and sequential number of tests that are required to generate a single threshold datum point representing an average of lowest (invariant) fracture loads. The large amount of data, based on approximately 700 individual tests for 36 material conditions, served as the basis for subsequent focused investigations on selected materials by (i) fractography, (ii) microstructural analysis, and (iii) hydrogen quantification experiments. The threshold data that were generated are the foundation for current and future work.

(a) No hydrogen added: hardness versus threshold tested in air (ISL_{air})

Quenched and tempered steel alloys contain a low concentration of residual hydrogen, located in either reversible or irreversible trap sites. For the alloys tested, this concentration is in the range of 1 ppm. Before testing the response of a material to an addition of hydrogen, the effect, if

Downloaded from https://royalsocietypublishing.org/ on 04 March 2022

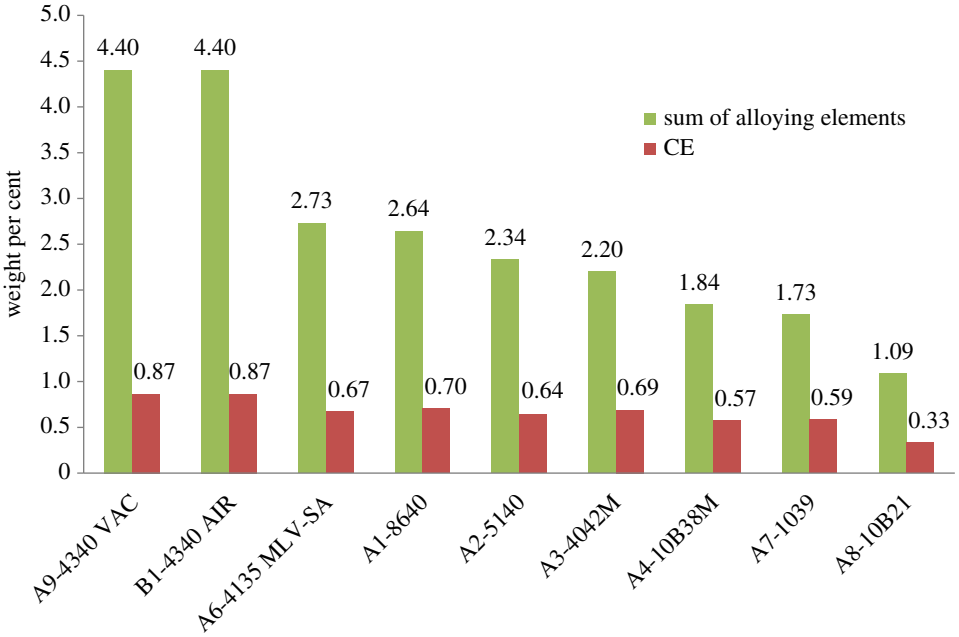

Figure 3. Sum of alloying elements and carbon equivalence (CE) for the alloys tested. Carbon equivalence, CE (wt%) $= C + Si/24 + Mn/6 + Cu/15 + Ni/12 + [Cr(1 - 0.016\sqrt{Cr})]/8 + Mo/4$ [22]. (Online version in colour.)

any, of residual hydrogen must be determined as a first step to establish baseline conditions. The measurement of HE threshold stress *in air* is the most immediate method of isolating the effect of residual hydrogen in a material. This measurement is achieved by performing a progressive incremental step loading (ISL) protocol in air on pristine samples to achieve the invariant (lowest) threshold load, ISL_{air}. The embrittlement ratio $NFS_{\%air}$ is a measure of the effect of residual hydrogen on the material.

Figure 4 illustrates average FF and ISL_{air} load values. At low hardness, FF and ISL_{air} are nearly identical. As hardness is increased, FF and ISL_{air} rise together, although a gap between the two conditions becomes more evident. The data, presented in figure 5 in terms of embrittlement ratio $NFS_{\%air}$, show a consistent trend whereby $NFS_{\%air}$ values decrease with increasing hardness from approximately 100% at low hardness to as low as 86% at 54 HRC. Previous studies with standard notch bars (i.e. made with AISI 4340 steel at 51–53 HRC) have shown a similar drop of $NFS_{\%air}$ to approximately 90%, presumed to be caused by residual hydrogen [2,3].

It must be emphasized that the decrease of relative fracture strength, $NFS_{\%air}$, is time-dependent. In other words, the effect is only apparent at very slow loading rates, which is consistent with the mechanism of hydrogen damage. Furthermore, increasing hardness results in progressively lower $NFS_{\%air}$ values, which is also consistent with the expected effect of rising hardness on HE susceptibility. These two points reinforce the idea that the observed decrease in $NFS_{\%air}$ is related to residual hydrogen, as opposed to an undefined effect of *creep* at ambient temperature.

Another aspect to consider is the effect of tempering temperature. Higher hardness is achieved by reducing temperature during tempering. Tempering also effectively *bakes out* hydrogen [23]; as tempering temperature is decreased, it stands to reason that less hydrogen is baked out. Therefore, it is very likely that higher-hardness samples obtained from the same alloy contain more residual hydrogen. This correlation between $NFS_{\%air}$ and tempering temperature is clearly observed in figure 6, which shows that $NFS_{\%air}$ increases with increasing tempering temperature.

In summary, the observed trend whereby $NFS_{\%air}$ decreases with increasing hardness is likely to be the result of two effects. As hardness is increased, (i) the material has greater susceptibility to hydrogen damage while also (ii) containing higher concentrations of residual hydrogen.

Downloaded from https://royalsocietypublishing.org/ on 04 March 2022

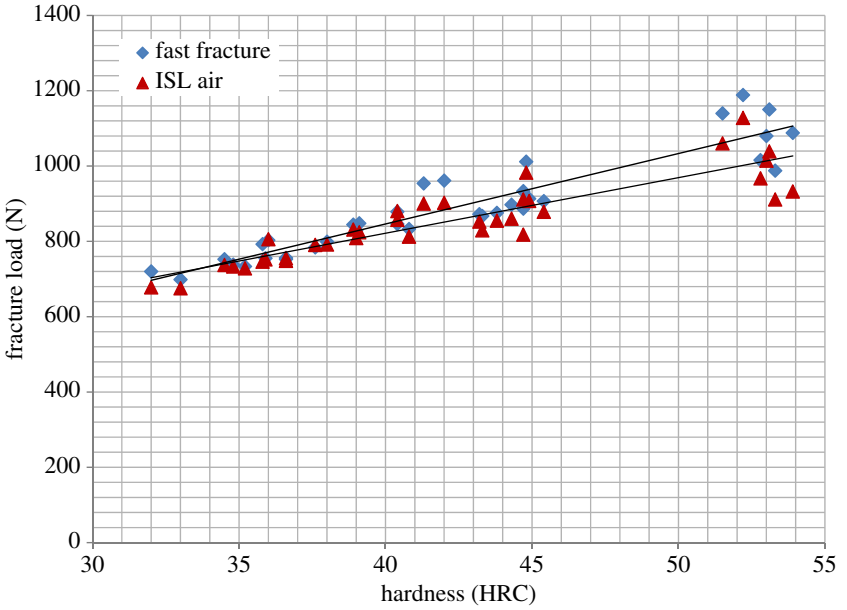

Figure 4. Average FF and ISL_{air} threshold loads tested in air under four-point bending load. Each data point represents an average of three to five samples tested. FF values obtained at loading rate of 445 N min^{-1}. ISL_{air} loading protocol: 2% NFS increments/2 h hold time until fracture or 5% drop in load. The loading rate was selected to generate the lowest (invariant) notch fracture strength at all levels of material hardness. (Online version in colour.)

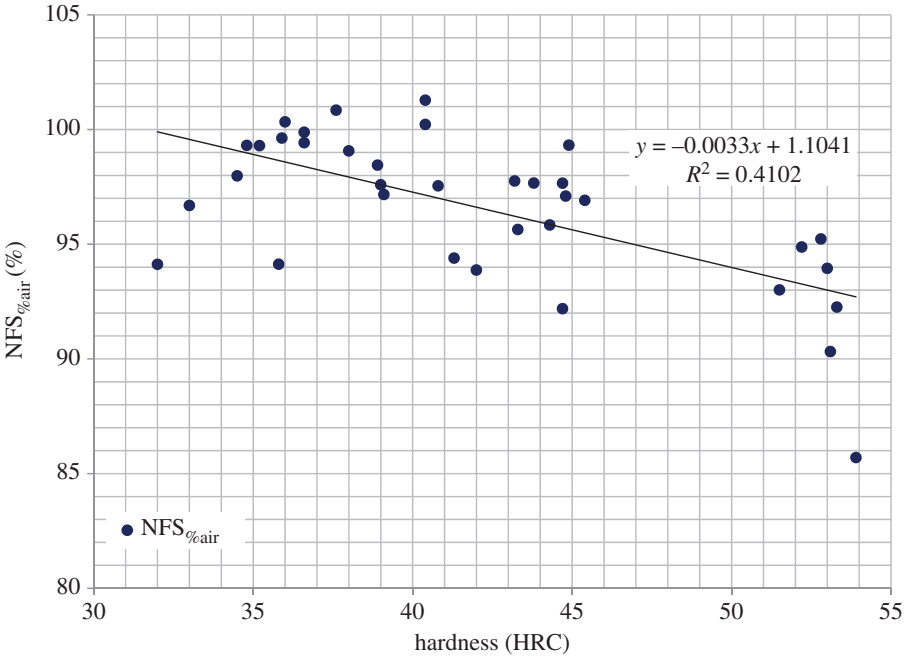

Figure 5. Embrittlement ratio $NFS_{\%air}$ shows a consistent trend whereby $NFS_{\%air}$ values decrease with increasing hardness. (Online version in colour.)

Downloaded from https://royalsocietypublishing.org/ on 04 March 2022

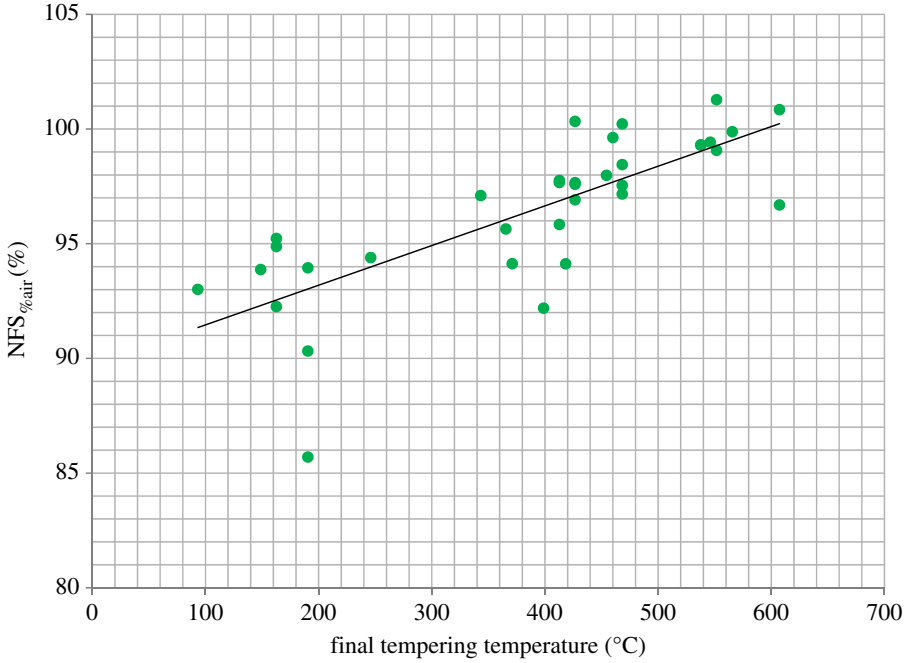

Figure 6. Correlation between $NFS_{\%air}$ and tempering temperature is clearly observed, which shows that $NFS_{\%air}$ increases with increasing tempering temperature. (Online version in colour.)

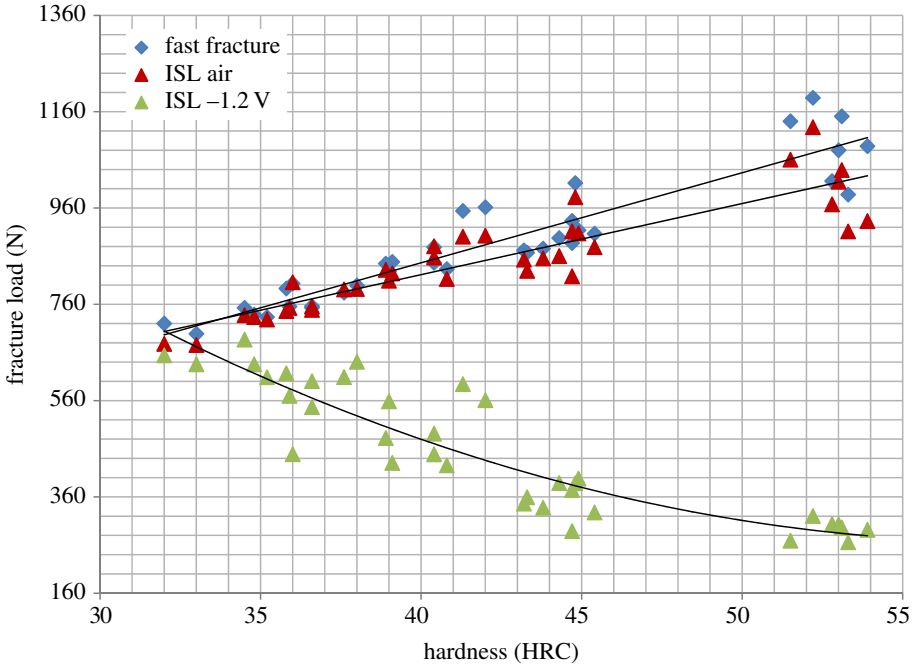

Figure 7. Average $ISL_{1.2V}$ threshold loads (juxtaposed onto FF and ISL_{air} results) tested at an imposed cathodic potential of −1.20 V under four-point bending load. Each data point represents an average of three to five samples tested. $ISL_{1.2V}$ loading protocol: 2% NFS increments/2 h hold time until fracture or 5% drop in load. The loading rate was selected to generate the lowest (invariant) notch fracture strength at all levels of material hardness. (Online version in colour.)

Downloaded from https://royalsocietypublishing.org/ on 04 March 2022

In all cases, the concentration of residual hydrogen is very low, which may explain why ISL_{air} continues to increase with increasing hardness, albeit at a slightly lower rate than FF. In other words, a small amount of hydrogen is not sufficient to cause a net loss of fracture strength. This observation raises the prospect that a *critical concentration of active hydrogen* must be reached for net loss of fracture strength to occur. The topic of critical hydrogen concentration will be revisited in the Discussion section (§4).

(b) Effect of environmental hydrogen charging: hardness versus threshold at imposed potential −1.20 V

Initial environmental tests were conducted on all materials under an imposed potential of −1.20 V. As was described in the Methodology section (§2a), this experimental condition is assumed to be representative of the worst-case naturally occurring galvanic corrosion condition. The expression $ISL_{1.2V}$ denotes the average of lowest (i.e. invariant) fracture load values obtained by using progressively slower ISL testing at an imposed potential of −1.20 V.

FF and $ISL_{1.2V}$ data for all alloys are illustrated as a function of hardness in figure 7, juxtaposed onto the previous ISL_{air} data. The data show a jaw-like trend whereby $ISL_{1.2V}$ threshold loads decrease with increasing hardness. This behaviour is consistent with HE phenomena. More precisely, in the current experimental configuration whereby a notched square bar is loaded in bending, loss of ductility and strength due to the presence of added hydrogen are also expected to cause a reduction of crack threshold in the notched sample. A notable observation is that the trend for $ISL_{1.2V}$ threshold is not linear. Rather, it appears to near a lower limit, whereby increasing hardness above 53 HRC does not appear to cause significantly lower threshold values. Stated otherwise, above 53 HRC the materials have reached a near-maximum degree of embrittlement.

These data validate the capability and sensitivity of the experimental set-up to provoke, detect and quantify HE even at low hardness levels, i.e. in the range of 35 HRC. The fact that quenched and tempered steel with hardness as low 35 HRC begins to exhibits a small but measurable degree of loss of fracture strength must be carefully considered in the context of the experimental conditions. These results were obtained under extreme experimental conditions of hydrogen concentration and stress applied in pure bending. The combination of these conditions is outside the normal spectrum for bolted joint applications, and therefore not directly applicable to mechanical fasteners without additional conversion and correlation, as will be discussed in the following section.

(c) Quantifying hydrogen embrittlement susceptibility: $NFS_{\%}$

The ratio $ISL_{1.2V}/FF$ expressed as $NFS_{\%1.2V}$ is a normalized measure of the HE susceptibility of the material, at a given concentration of hydrogen absorbed during the experiment, precisely under an imposed cathodic potential of −1.20 V. Figure 8 illustrates the data in terms of $NFS_{\%1.2V}$. The highest-hardness group, 53 HRC, achieved average $NFS_{\%1.2V}$ values below 30%, reaching as low as 23.6% for alloy A6 (AISI 4135 MLV). Such low $NFS_{\%1.2V}$ values are indicative of a very high degree of embrittlement, reflective of the severity of the experimental conditions in terms of both hydrogen concentration and stress. This degree of susceptibility also appears to be at the bottom limit, whereby increasing hardness above 53 HRC does not cause significantly lower threshold values. It can be anticipated that higher imposed potentials (e.g. −1.00 V) resulting in less absorbed hydrogen would cause the threshold curve in figure 8 to trend upwards, reflecting a lower degree of embrittlement.

An important engineering analysis is to examine the data in the context of acceptance threshold for fastener applications where a bolt or screw is loaded in tension. By applying the acceptance level of 60% NFS in bending, equivalent to 100% in tension per ASTM F2660 [24], it can be seen that the convention of using 39 HRC (approx. 390 HV, 1200 MPa) as the specified hardness limit for acceptable HE susceptibility holds true, even under the most severe hydrogen charging condition.

Downloaded from https://royalsocietypublishing.org/ on 04 March 2022

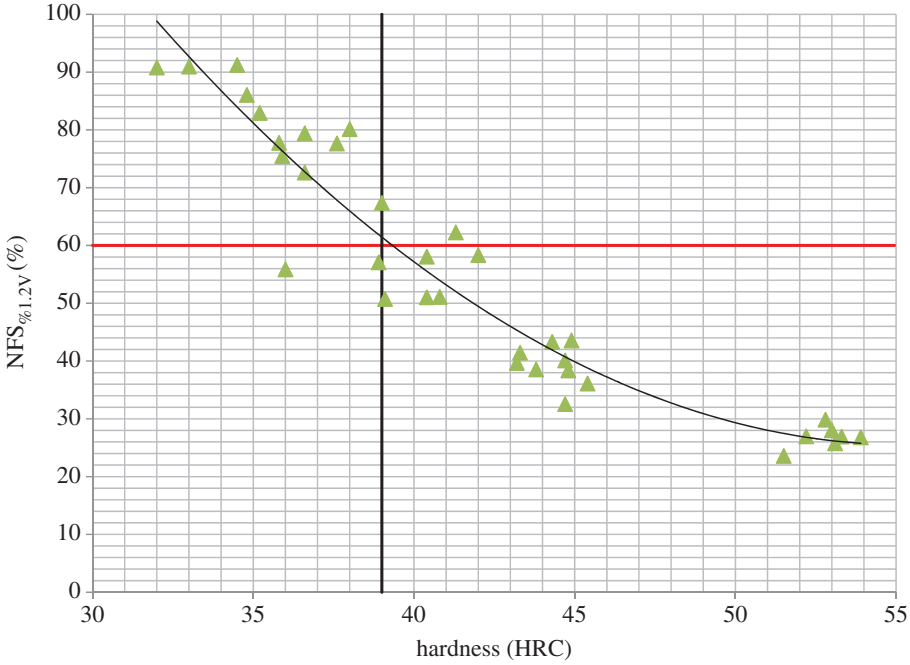

Figure 8. Embrittlement ratio $NFS_{\%1.2V}$ show a consistent trend whereby $NFS_{\%1.2V}$ values decrease with increasing hardness. Note that the 60% line represents the limit of acceptability for fasteners. (Online version in colour.)

It should be noted that 39 HRC (390 HV) is the maximum specified hardness for externally threaded fasteners with tensile strength ranging from 1000 to 1200 MPa (150–175 ksi) such as ISO 898-1 property class 10.9 [25] and SAE J429 grade 8 [26].

(d) Threshold analysis segregated by alloy

The $NFS_{\%1.2V}$ results shown previously are identified by alloy (figure 9). When segregated by alloy, the threshold load values $ISL_{1.2V}$ can be readily fitted to second-order polynomial curves that are unique to each alloy, as shown in two examples (figures 10 and 11). In other words, the HE threshold data show variation that is alloy-specific, which is attributable to the effect of sub-microstructure on H transport and trapping. More precisely, the data are fundamentally a reflection of the ability for H to be available and to accumulate at points of stress concentration and eventually to participate in the damage mechanism; in other words, to be 'active'. Closer examination of these data is presented along several themes.

(i) Theme 1: most and least susceptible materials

The first and most important theme of interest is to find trends that indicate which, if any, materials are most or least susceptible. This question is evaluated in the context of two regimes: (i) low hardness, comprising the 35 and 39 HRC groups, and (ii) high hardness, comprising 45 and 53 HRC groups.

In the low-hardness regime, two alloys consistently represent upper and lower $NFS_{\%1.2V}$ boundaries. Alloy A1-8640H exhibits the lowest $NFS_{\%1.2V}$ values, whereas alloy B1-4340-AirMelt exhibits the highest $NFS_{\%1.2V}$ values (figure 12). By extrapolation, the difference between the two alloys can reach as high as 22% $NFS_{\%1.2V}$, which is a large difference in susceptibility.

In the high-hardness regime, alloy A6-4135MLV exhibits the lowest $NFS_{\%1.2V}$ values, whereas alloy A2-5140 exhibits the highest $NFS_{\%1.2V}$ values (figure 13). By extrapolation, the difference

Downloaded from https://royalsocietypublishing.org/ on 04 March 2022

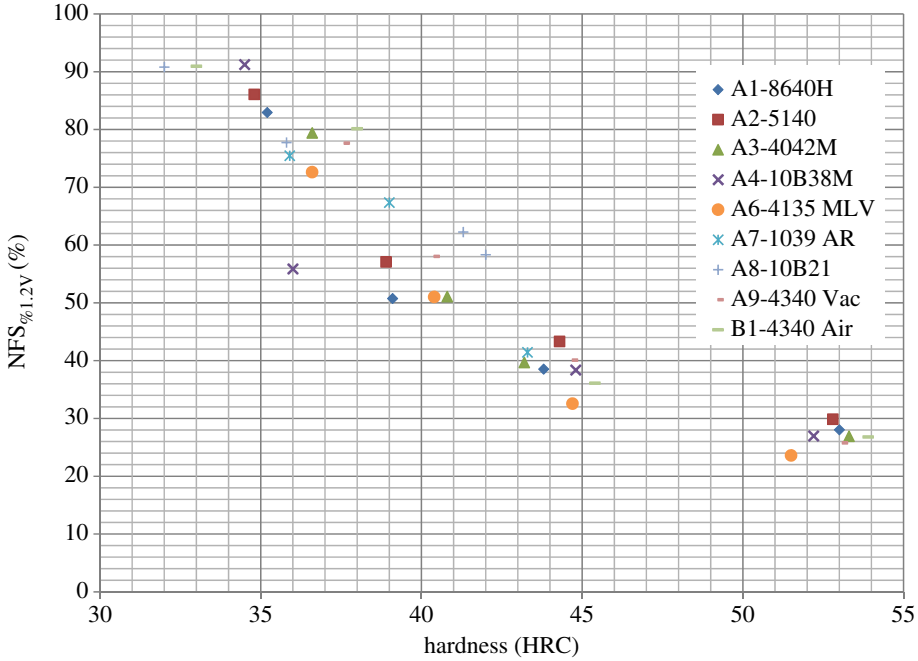

Figure 9. Embrittlement ratio $NFS_{\%1.2V}$ segregated by alloy. (Online version in colour.)

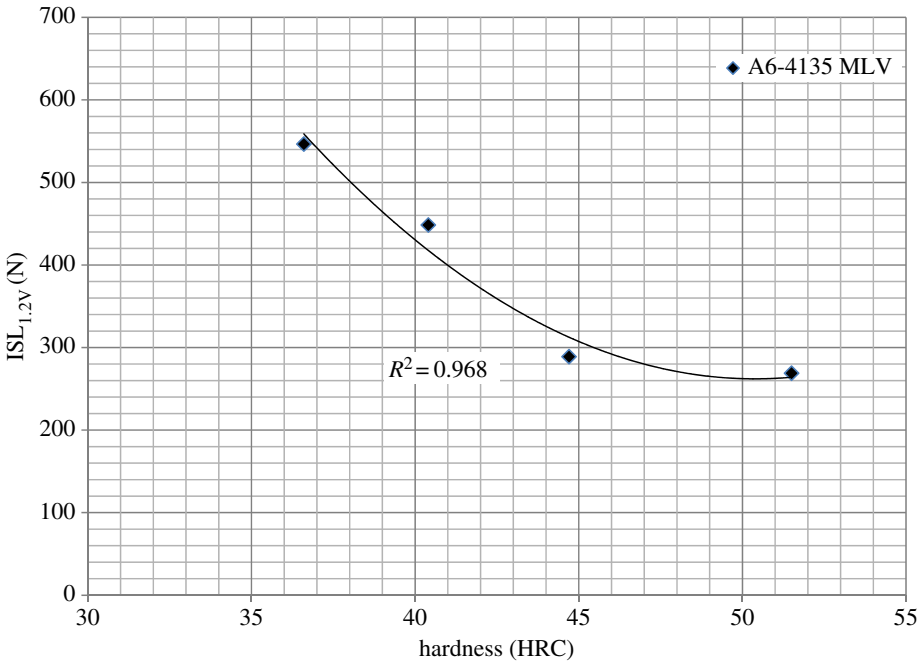

Figure 10. Embrittlement ratio $NFS_{\%1.2V}$ for alloy A6-4135 MLV. (Online version in colour.)

between the two alloys can reach as high as 10% $NFS_{\%1.2V}$, which is also a significant difference in susceptibility. The trend observed with these two alloys in the high-hardness regime is also apparent, albeit to a lesser extent, in the low-hardness regime. These two alloys are taken to represent boundaries for HE susceptibility in quenched and tempered martensitic steels commonly used for fasteners.

Downloaded from https://royalsocietypublishing.org/ on 04 March 2022

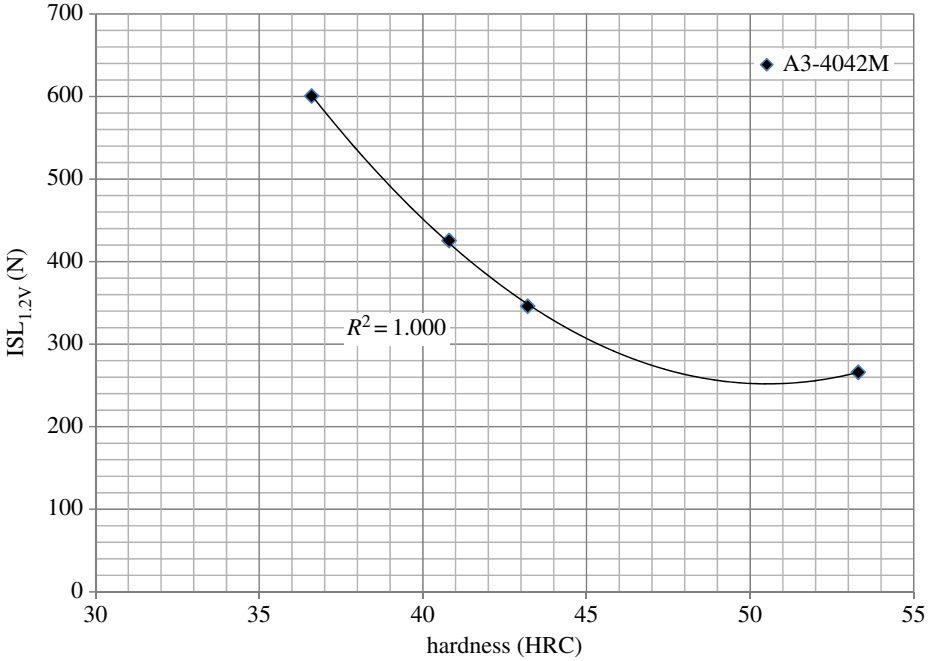

Figure 11. Embrittlement ratio $NFS_{\%1.2V}$ for alloy A3-4042 M. (Online version in colour.)

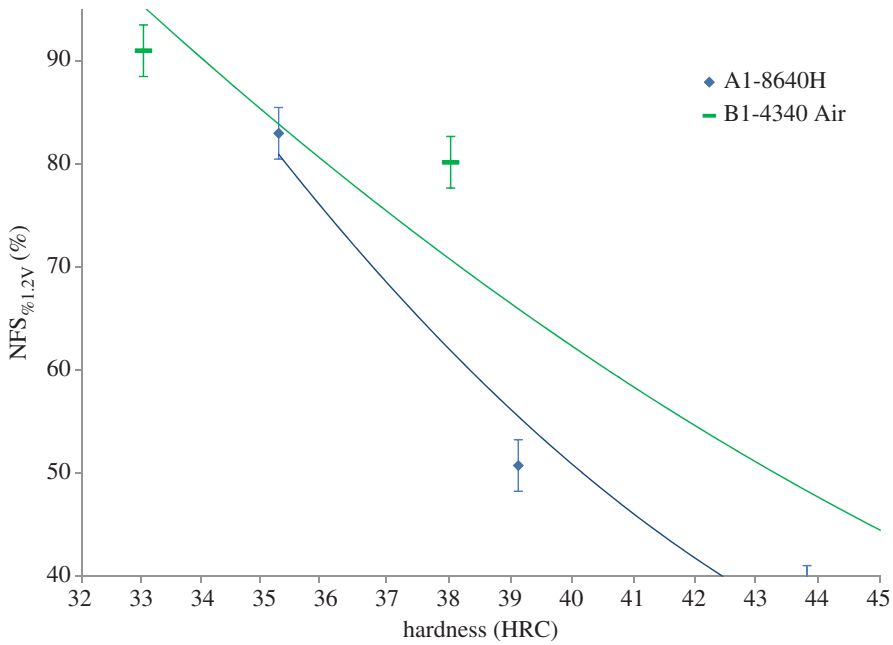

Figure 12. In the low-hardness regime, two alloys consistently represent upper and lower $NFS_{\%1.2V}$ boundaries. Alloy A1-8640H exhibits the lowest $NFS_{\%1.2V}$ values, whereas alloy B1-4340-AirMelt exhibits the highest $NFS_{\%1.2V}$ values. By extrapolation, the difference between the two alloys can reach as high as 22% $NFS_{\%1.2V}$, which is a large difference in susceptibility. (Online version in colour.)

(ii) Theme 2: carbon–boron steels

A second theme is the performance of carbon–boron microalloyed steels, which are very popular with fastener manufacturers. Carbon–boron microalloyed steels offer the dual benefit of

Downloaded from https://royalsocietypublishing.org/ on 04 March 2022

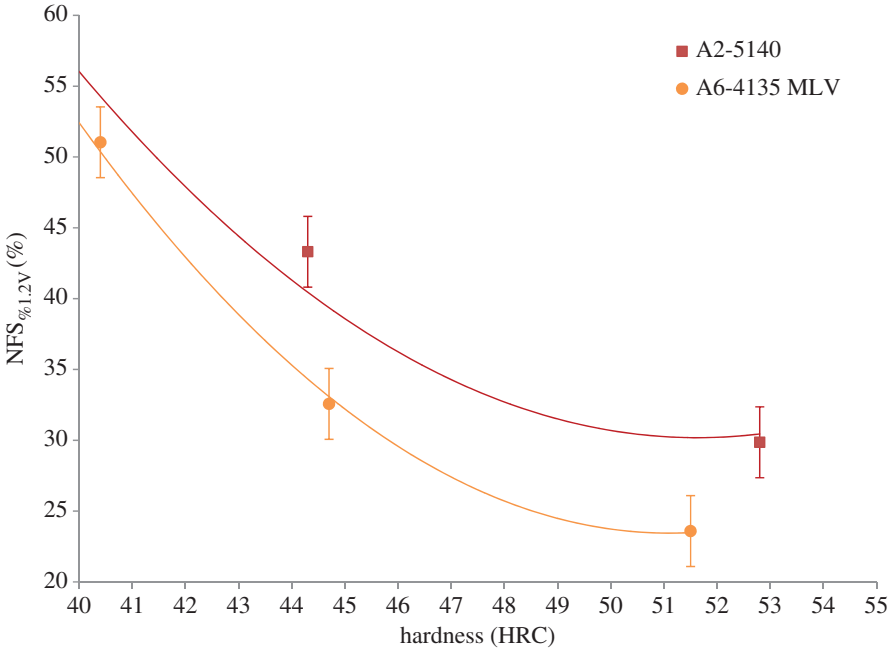

Figure 13. In the high-hardness regime, alloy A6-4135MLV exhibits the lowest $NFS_{\%1.2V}$ values, whereas alloy A2-5140 exhibits the highest $NFS_{\%1.2V}$ values. By extrapolation, the difference between the two alloys can reach as high as 10% $NFS_{\%1.2V}$, which is also a significant difference in susceptibility. (Online version in colour.)

improved formability by reducing carbon while also enhancing hardenability, thus compensating for lower carbon [27,28]. The addition of a significant concentration of hydrogen does not reveal any obvious difference in $NFS_{\%1.2V}$ between alloy A8-10B21 and other alloys. This observation is explained by the high concentration of hydrogen under cathodic charging. In such conditions, where the material is effectively being saturated with hydrogen, any difference in initial residual hydrogen concentration is comparatively negligible.

It should be noted that the results for alloy A8-10B21 are limited by the fact that samples could not be produced at hardness above 42 HRC. This hardness limit due to the lower carbon content also means that A8-10B21 samples produced at 42 HRC (M29, M30) are in the near-as-quenched condition. In other words, they have not undergone any significant degree of tempering. It is, therefore, reasonable to assume that these materials are characterized by higher dislocation densities than for other alloys at similar hardness. On the other hand, they are also likely to be characterized by lower carbide precipitate volume fractions due to (i) absence of tempering and (ii) absence of alloying elements. From this analysis, it can be stated that the effects of tempering, notably dislocation reduction followed by precipitation, when considered in isolation from other factors, are not sufficient to predict either an increase or a decrease in HE susceptibility.

Alloy A4-10B38 is a carbon–boron steel similar to A8-10B21, but with nearly double the carbon concentration. Despite the higher carbon concentration and correspondingly higher hardness, the absence of alloying elements means that tempered A4-10B38 contains only cementite and no other carbides. This characteristic of A4-10B38 has not produced any perceptible difference, for better or worse, in HE susceptibility. With the exception of an apparent outlier at 36 HRC (M6), the threshold curve for A4-10B38 is indistinguishable from the bulk of the other alloys.

(iii) Theme 3: chemical composition and carbon equivalence

A fundamental question is whether it is possible to distinguish the presumed effect of microstructure, the complex result of composition and heat treatment, from the effect of

Downloaded from https://royalsocietypublishing.org/ on 04 March 2022

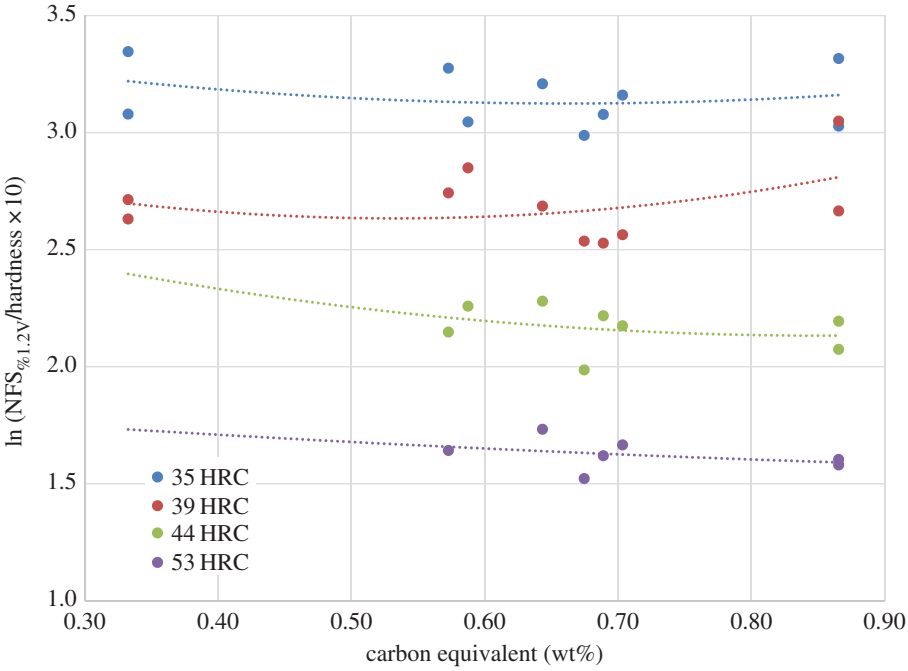

Figure 14. HE_n is a normalized hydrogen embrittlement ratio. The results for CE versus HE_n do not show any clear trend of changing susceptibility with increasing carbon equivalence. (Online version in colour.)

composition alone. In describing the results thus far, it is presumed that differences in microstructure have a second-order effect on HE susceptibility. Yet, a clear effect of microstructure has not been established. On the other hand, the analysis has shown a direct effect linked to differences in composition. Therefore, it is necessary to examine the effect of composition alone before addressing microstructure.

The total alloy content and carbon equivalent values for the steel grades included in this study are illustrated in decreasing order in figure 3. From this chart, it can be seen that the 4340 has the highest alloy content (4.4 wt%) and the highest CE (0.87 wt%). The other alloy steels, A6-4135, A1-8640, A2-5140 and A3-4042, all have similar CE values, ranging from 0.64 to 0.70 wt%. The non-alloyed steels have the lowest CE values. Plain carbon A7-1039 and carbon–boron A4-10B38 have similar CE values, 0.59 and 0.57 wt%, respectively. Low-carbon A8-10B21 has the lowest CE at 0.33 wt%. It should be noted that the formulae for CE do not account for the hardenability effect of boron, which is considered a microalloying additive.

In order to determine if chemical composition, expressed as CE, has a direct effect on HE susceptibility, one approach is to plot CE versus $NFS_{\%1.2V}$ for each of the four hardness groups. However, given that, within each hardness group, small differences in hardness may have an impact on $NFS_{\%1.2V}$, an attempt was made to normalize for hardness. An empirically derived expression for HE susceptibility is

$$HE_n = \ln \frac{NFS_{\%1.2V}}{HRC \times 10}, \tag{3.1}$$

where the expression HE_n represents a normalized HE ratio that follows $NFS_{\%1.2V}$. In other words, when $NFS_{\%1.2V}$ increases, so does HE_n. The results for CE versus HE_n (figure 14) do not show any clear trend of changing susceptibility with increasing carbon equivalence. To further explore this observation, the effect of alloying elements on hydrogen transport and trapping is examined from the literature. It is reported that alloying elements do not have a direct effect on the diffusion process, as they do not alter the kinetics of diffusion in martensite [23]. On the other

Downloaded from https://royalsocietypublishing.org/ on 04 March 2022

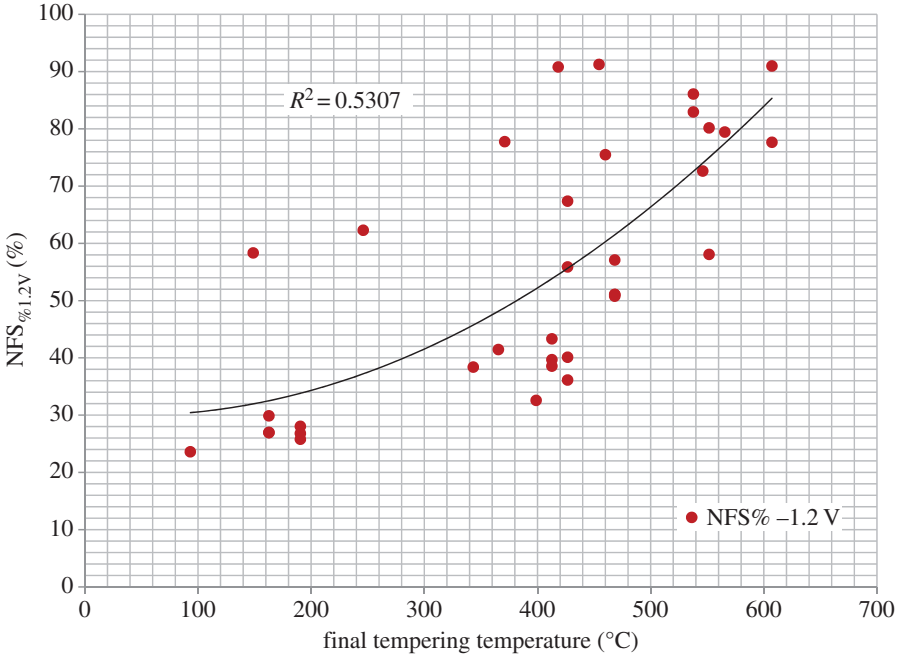

Figure 15. A trend of lower $NFS_{\%1.2V}$ is observed with decreasing tempering temperature; however, tempering temperature does not have a direct effect on HE susceptibility, which explains the poor data fit. (Online version in colour.)

hand, there is evidence that they have an indirect role on trapping, resulting in a decrease of the effective diffusion coefficient with increasing carbon equivalent [22,23]. Hinotani *et al*. showed that increasing carbon resulted in an increase of trap sites [29]. The increase in carbon causes distortion of the lattice, which in turn generates dislocations, considered preferential trap sites. An increase in the number of trap sites can cause a decrease of the effective diffusion coefficient.

In summary, although there is reason to believe that composition can affect hydrogen transport and trapping, notably by reduction in diffusion rate with increasing CE, the results of this study show no obvious effect of CE on HE susceptibility. Although there is not an obvious explanation, it is possible that, at an imposed potential of −1.20 V, the lattice and dislocations are saturated with H relatively quickly, thus negating any measurable effect of increased dislocation density on hydrogen transport, and on observed HE susceptibility.

(iv) Theme 4: effect of tempering temperature

As was mentioned at the outset, hardness has a first-order effect on HE susceptibility. Higher hardness is achieved by reducing the temperature during tempering. Therefore, it is normal that a trend of lower $NFS_{\%1.2V}$ is observed with decreasing tempering temperature as shown in figure 15. However, the data points show a poor fit to the binomial trend line. This poor fit is explained by the fact that tempering temperature does not have a direct effect on HE susceptibility. Rather, tempering temperature determines the final as-tempered microstructure, which in turn has second-order effects on hydrogen damage and transport and trapping mechanisms.

4. Discussion

(a) Threshold curve

Threshold results presented thus far were obtained under a single hydrogen charging condition (i.e. −1.20 V). There is significant value to performing ISL testing while systematically varying

Downloaded from https://royalsocietypublishing.org/ on 04 March 2022

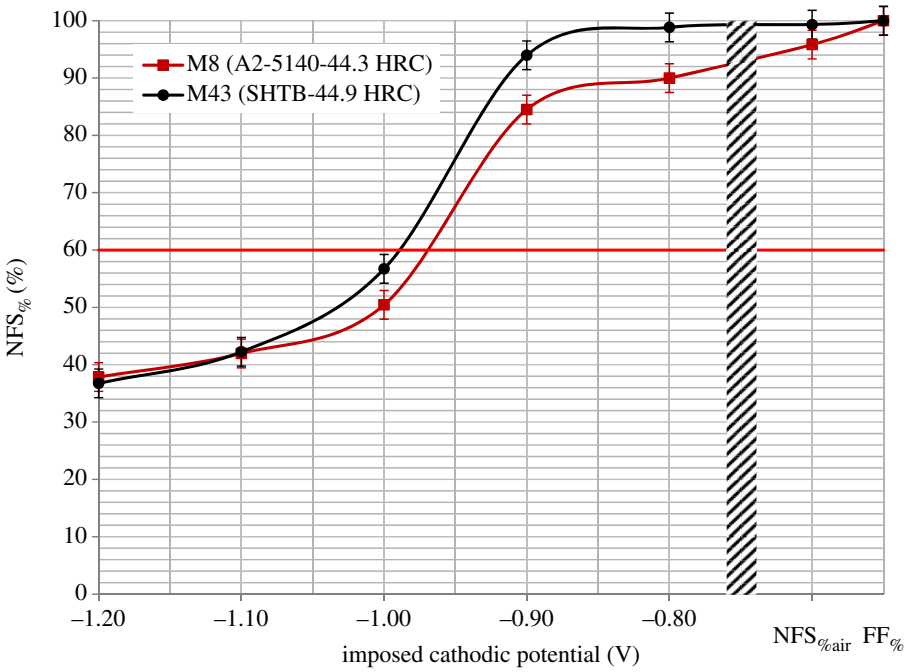

Figure 16. Full *threshold curve*, depicting $NFS_{\%}$ versus imposed potential, for a material condition (i.e. alloy + hardness) at the full range of hydrogen charging conditions characterized by a ductile–brittle transition between −0.9 V and −1.0 V. In this figure, alloy M8 (A2-5140-44.3 HRC) is compared with an experimental alloy (SHTB-44.9) comprising intentional VC precipitates as hydrogen traps. The threshold curves illustrate that the SHTB-44.9 is measurably less susceptible to hydrogen embrittlement. (Online version in colour.)

hydrogen charging conditions. More precisely, this approach requires decreasing added hydrogen by increasing the imposed potential (e.g. −1.10 V to −0.70 V). The compiled results may be used to generate a full *threshold curve*, depicting $NFS_{\%}$ versus imposed potential, for a material condition (i.e. alloy + hardness). The HE threshold curve defines the characteristic behaviour of a material at the full range of hydrogen charging conditions. Sample threshold curves for two alloys at 45 HRC are shown in figure 16. HE threshold curves are sigmoidal in shape, characterized by a ductile–brittle transition. In figure 16, the ductile–brittle transition occurs between −0.90 V and −1.00 V and is triggered by increasing the concentration of hydrogen. This transition illustrates that a *critical concentration of hydrogen* is required to promote the hydrogen damage mechanism causing a normally ductile material to become brittle. Less-susceptible materials are characterized by ductile–brittle transitions that are further to the left. In other words, a lower *critical concentration of hydrogen* is required to trigger the ductile–brittle transition. Each material condition (i.e. alloy + hardness) has its own signature HE threshold curve that can only be determined experimentally.

Threshold curves can serve a number of important scientific and engineering purposes. When used as a performance metric, threshold curves can be juxtaposed to compare the HE susceptibility of two alloys at equal hardness. This approach may be used to select an engineering material on the basis of minimizing HE susceptibility. When used as a technical tool, threshold curves can guide the development of more resistant alloys by quantifying the impact of modulating microstructure characteristics, such as grain size, dislocation density and precipitates, on HE susceptibility of a bulk material. When used as a scientific tool, threshold curves can help validate the fundamental basis for explaining the transport and trapping interaction of hydrogen in a bulk material.

It can take several months of testing to fully generate a threshold curve for a single material condition. Consequently, not all 36 material conditions can reasonably be tested in this way.

Downloaded from https://royalsocietypublishing.org/ on 04 March 2022

Rather, only a few alloys, at all four hardness conditions, will be selected judiciously as part of future work for full threshold curve determination.

(b) Effect of microstructure

Attempts at engineering HE-resistant microstructures have achieved varying degrees of success. For example, the introduction of vanadium carbide precipitates has shown some promise, as shown in figure 16, by increasing the trap density in the material [18,30]. The use of bainitic structures obtained by austempering has also shown a marginal decrease in susceptibility by slowing hydrogen diffusion [31]. The challenge in this study is that the microstructures are fundamentally the same, with only minor differences, which can only be resolved by advanced characterization.

Measurement of threshold stress by incremental step load testing showed that, in the higher hardness range, alloy A6-4135MLV exhibits the lowest $NFS_{\%1.2V}$ values, whereas alloy A2-5140 exhibits the highest $NFS_{\%1.2V}$ values. These two alloys are taken to represent the limits of HE susceptibility in quenched and tempered martensitic steels commonly used for fasteners. However, the results do not provide insight into hydrogen transport and trapping characteristics of the materials. It is, therefore, necessary to conduct a detailed analysis and comparison of the microstructures. The two alloys, A6-4135MLV and A2-5140, were selected for in-depth multiscale microstructural analysis. Each alloy was examined at the highest hardness (approx. 53 HRC) representing the quasi-as-quenched condition and at the lowest hardness (approx. 35 HRC) representing the most tempered condition. The details of the microstructural analysis are the topic of another paper; however, a summary of findings is provided in the electronic supplementary material.

Thus far, the microstructural analysis has not led to identifying specific characteristics or features that correlate directly with the differences in HE threshold. Given the close similarities between the microstructures, further compilation of analyses, including stress–strain behaviour, of these and other martensitic materials is required. The microstructural analyses are also being supplemented with hydrogen measurement techniques, notably thermal desorption spectroscopy to characterize hydrogen trapping and electrochemical permeation to measure effective hydrogen diffusion rates.

5. Conclusion

The results of this extensive study confirm the first-order effect of hardness/strength on HE susceptibility. More specifically, it was shown that, under extreme conditions of bending stress and hydrogen charging, loss of fracture strength begins at approximately 35 HRC and tends towards a minimum above 55 HRC. When the stress intensity in bending is converted to match a fastener's tensile stress condition, even under extreme experimental hydrogen charging conditions, the critical hardness below which the material would remain unaffected is 39 HRC, a finding that is consistent with the current direction in consensus fastener standards. The results have also illustrated a second-order effect that is consistently specific to each alloy. More precisely, tempered martensites produced at equal hardness from different steel alloys consistently exhibit second-order differences in HE susceptibility. It was also demonstrated that the alloy dependence of the results is related not to composition alone, but likely to microstructure, which is the combined outcome of composition and heat treatment. A plausible explanation is that differences in sub-microstructure characteristics influence both stress–strain behaviour and hydrogen transport and trapping, and consequently also influence susceptibility. However, given the close similarities between the martensitic microstructures of the common fastener materials investigated here, detailed multiscale analysis of the microstructures has not yet identified specific characteristics or features that correlate directly with the differences in HE threshold. Identifying these characteristics is the subject of current and future work. The engineering and scientific implications of this work include establishing a roadmap for selecting

Downloaded from https://royalsocietypublishing.org/ on 04 March 2022

materials that exhibit greater HE resistance and for developing new alloys with improved HE resistance.

Data accessibility. Data on heat treatment conditions of each material and a summary of microstructure analyses are provided in the electronic supplementary material.

Authors' contributions. S.V.B. conceived and performed the study as part of his PhD thesis under the advisement of S.Y. Portions of experimental work were performed by K.R.S., who also assisted with data compilation and analysis.

Competing interests. We declare we have no competing interests.

Funding. Research on fastener hydrogen embrittlement at McGill University in Montreal, Canada, began in 2006 as a collaborative effort, co-sponsored by industry and the Government of Canada through the Natural Sciences and Engineering Research Council (NSERC). Industrial partnership was led by the Industrial Fasteners Institute (IFI), the Canadian Fasteners Institute (CFI), Boeing, Infasco, Nucor Fasteners, the Research Council on Structural Connections (RCSC) and ASTM Committee F16.96 on Bolting Technology. The ongoing research follows two distinct tracks: (i) fastener materials susceptibility to HE and (ii) interactions of fastener materials with coatings and coating processes.

Acknowledgment. The authors thank Arya Fatehi (McGill University) for his assistance with experimental parts of this work.

References

1. ISO. 2014 *ISO-1891-2:2014-3.4.9 Fasteners—terminology—part 2: vocabulary and definitions for coatings*. Geneva, Switzerland: International Organization for Standardization (ISO).
2. Brahimi S. 2007 Effect of surface processing variables on hydrogen embrittlement of steel fasteners. ME thesis, McGill University, Montreal, Quebec, Canada.
3. Brahimi S, Yue S. 2009 Effect of surface processing variables and coating characteristics on hydrogen embrittlement of steel fasteners. Part 2: Electroplating and non electrolytic processes. Presented at *National Association for Surface Finishing Annual Technical Conf. 2009* (*SUR/FIN 2009*), *Louisville, KY, 16–17 June*.
4. Oriani RA. 1978 Hydrogen embrittlement of steels. *Annu. Rev. Mater. Sci.* **8**, 327–357. (doi:10.1146/annurev.ms.08.080178.001551)
5. Oriani RA, Hirth JP, Smialowski M. 1985 *Hydrogen degradation of ferrous alloys*. Park Ridge, NJ: William Andrew/Noyes.
6. Oriani RA. 1972 A mechanistic theory of hydrogen embrittlement of steels. *Ber. Bunsenges. Phys. Chem.* **76**, 848–857. (doi:10.1002/bbpc.19720760864)
7. Pfeil LB. 1926 The effect of occluded hydrogen on the tensile strength of iron. *Proc. R. Soc. Lond. A* **112**, 182–195. (doi:10.1098/rspa.1926.0103)
8. Beachem CD. 1972 A new model for hydrogen-assisted cracking (hydrogen 'embrittlement'). *Metall. Trans.* **3**, 441–455. (doi:10.1007/bf02642048)
9. Birnbaum HK, Sofronis P. 1994 Hydrogen-enhanced localized plasticity—a mechanism for hydrogen-related fracture. *Mater. Sci. Eng. A* **176**, 191–202. (doi:10.1016/0921-5093(94)90975-X)
10. Song J, Curtin WA. 2013 Atomic mechanism and prediction of hydrogen embrittlement in iron. *Nat. Mater.* **12**, 145–151. (doi:10.1038/nmat3479)
11. Lee J-Y, Lee J-L. 1987 A trapping theory of hydrogen in pure iron. *Philos. Mag. A* **56**, 293–309. (doi:10.1080/01418618708214387)
12. Oriani RA. 1970 The diffusion and trapping of hydrogen in steel. *Acta Metall.* **18**, 147–157. (doi:10.1016/0001-6160(70)90078-7)
13. Brahimi S, Sriraman K, Yue S. In press. Hydrogen embrittlement characteristics of two tempered martensitic steel alloys for high-strength bolting. *Proc. Inst. Mech. Engrs, Part C: J. Mech. Engg Sci.* online. (doi:10.1177/0954406216642476)
14. ISO. 2017 (Expected) *ISO/TR 20491 Fundamentals of hydrogen embrittlement in steel fasteners*. Geneva, Switzerland: International Organization for Standardization (ISO).
15. Brahimi S. 2014 *Fundamentals of hydrogen embrittlement in steel fasteners*. Cleveland, OH: Industrial Fasteners Institute (IFI).
16. Brahimi S, Aguilar R, Christensen C. 2013 *Metallurgical analysis of Bay Bridge broken anchor rods S1-G1 & S2-A6*. Joint Project Report, California Department of Transportation – American Bridge Fluor, 7 May. See http://baybridgeinfo.org/sites/default/files/pdf/E2%20Shear%20Key%20Rod%20Failure%20Fracture%20Analysis%20Report_5.7.13.pdf.

Downloaded from https://royalsocietypublishing.org/ on 04 March 2022

17. Pressouyre GM, Bernstein IM. 1978 A quantitative analysis of hydrogen trapping. *Metall. Trans. A* **9**, 1571–1580. (doi:10.1007/bf02661939)
18. Yamasaki S, Bhadeshia HK. 2006 M_4C_3 precipitation in Fe–C–Mo–V steels and relationship to hydrogen trapping. *Proc. R. Soc. A* **462**, 2315–2330. (doi:10.1098/rspa.2006.1688)
19. Das T. 2016 Hydrogen embrittlement susceptibility of high strength tempered martensite steels. ME thesis, McGill University, Montreal, Quebec, Canada.
20. ISO. 2012 *ASTM F1624-12 Standard test method for measurement of hydrogen embrittlement threshold in steel by the incremental step loading technique*. West Conshohocken, PA: ASTM International.
21. ISO. 2010 *ASTM F519-10 Standard test method for mechanical hydrogen embrittlement evaluation of plating/coating processes and service environments*. West Conshohocken, PA: ASTM International.
22. Yurioka N, Okumura M, Kasuya T, Cotton H. 1987 Prediction of HAZ hardness of transformable steels. *Met. Constr.* **19**, 217.
23. Frappart S, Oudriss A, Feaugas X, Creus J, Bouhattate J, Thébault F, Delattre L, Marchebois H. 2011 Hydrogen trapping in martensitic steel investigated using electrochemical permeation and thermal desorption spectroscopy. *Scr. Mater.* **65**, 859–862. (doi:10.1016/j.scriptamat.2011.07.042)
24. ASTM. 2013 *ASTM F2660-13 Standard test method for qualifying coatings for use on A490 structural bolts relative to environmental hydrogen embrittlement*. West Conshohocken, PA: ASTM International.
25. ISO. 2013 *ISO-898-1:2013 Mechanical properties of fasteners made of carbon steel and alloy steel — part 1: bolts, screws and studs with specified property classes—coarse thread and fine pitch thread*. Geneva, Switzerland: International Organization for Standardization (ISO).
26. SAE. 2014 *SAE J429-2014 Mechanical and material requirements for externally threaded fasteners*. Warrendale, PA: SAE International.
27. Grange R, Mitchell J. 1961 On the hardenability effect of boron in steel. *Trans. Am. Soc. Metals* **53**, 157–180.
28. Melloy G, Slimmon P, Podgursky P. 1973 Optimizing the boron effect. *Metall. Trans.* **4**, 2279–2289. (doi:10.1007/BF02669367)
29. Hinotani S, Ohmori Y. 1985 Effect of carbon content on the hydrogen diffusion in cold worked iron. *Trans. Jpn Inst. Metals* **26**, 622–629. (doi:10.2320/matertrans1960.26.622)
30. Park GT, Koh SU, Jung HG, Kim KY. 2008 Effect of microstructure on the hydrogen trapping efficiency and hydrogen induced cracking of linepipe steel. *Corros. Sci.* **50**, 1865–1871. (doi:10.1016/j.corsci.2008.03.007)
31. Saliby F, Brahimi S, Yue S. 2015 *Hydrogen embrittlement susceptibility of bainite for high strength steel fasteners*. Cleveland, OH: Industrial Fasteners Institute (IFI).